



2nd Advanced Optical Metrology Compendium

Advanced Optical Metrology

Geoscience | Corrosion | Particles | Additive Manufacturing: Metallurgy, Cut Analysis & Porosity



EVIDENT
OLYMPUS

WILEY

The latest eBook from **Advanced Optical Metrology**.
Download for free.

This compendium includes a collection of optical metrology papers, a repository of teaching materials, and instructions on how to publish scientific achievements.

With the aim of improving communication between fundamental research and industrial applications in the field of optical metrology we have collected and organized existing information and made it more accessible and useful for researchers and practitioners.

EVIDENT
OLYMPUS

WILEY

Structural Evolution of C₆₀ Molecular Crystal Predicted by Neural Network Potential

Kun Ni,* Fei Pan, and Yanwu Zhu*

The preparation of fullerene and a wide range of derivatives has attracted much attention in past decades. Understanding the structural evolution starting from fullerene is critical to guide the experimental exploration but has been paid less attention yet. Using *ab initio* molecular dynamics or global structural search algorithm accompanied with density functional theory calculations can give a glance of the potential energy surface (PES), but suffers high cost and low efficiency. Herein, by using neural network potentials and stochastic surface walking global structural search method, an accelerated energy calculation, and the higher efficient PES mapping starting from C₆₀ molecular crystal are reported. The structural evolution is found to follow an order of molecular crystal → polymers → opened caged ordered structures → 3D) curved carbon and graphite under zero pressure. Under high pressures, e.g., 50 GPa, the evolution follows a pathway of fullerene → sp² and sp³ hybrid carbon → sp³ amorphous carbon and crystal diamond. The electronic property calculation of the obtained structures in the evolution pathway shows a band gap depending on the order parameter of the generated structures, suggesting that more novel carbons can be potentially prepared in experiments, starting from C₆₀.

shows a face-centered cubic (fcc) structure under ambient conditions, and can be transformed into simple cubic structure below 250 K^[3] or into a close-packed hexagonal structure by recrystallization of C₆₀ from benzene at room temperature.^[4] When being applied simultaneously with a pressure of 3 to 8 GPa and heating at 573 ~ 973 K,^[5] irritated by an electron^[6] or photon beam,^[7] or doped by alkali metals,^[8] part of carbon atoms in C₆₀ may transform into sp³ hybridization via 2 + 2 cycloaddition reaction, forming fullerene polymers,^[9] in which the electronic structure is sensitive to the periodicity.^[10] When C₆₀ cages were confined in carbon nanotubes and subject to heating at 923 K in a vacuum, a peapod-like structure was reported showing the negative curvature in the connection region between cages.^[11] This could open a door for the construction of Schwarzite carbons, which have been considered as negative-curvature analogs of fullerenes.^[12]

1. Introduction

Fullerene C₆₀, as a zero-dimensional spherical structure consisting of 60 carbon atoms arranged in 20 hexagons and 12 pentagons, has attracted a broaden interest in the past few decades and triggered more research on its 1D counterpart, carbon nanotubes, and 2D counterpart, graphene. With a well-defined cage structure and unique physical properties,^[1] C₆₀ can act as a building block or a precursor for constructing new carbons, which often show features depending on the ordering of cages and interactions between cages. Such a design paradigm based on C₆₀ molecules could lead to novel optical, mechanical, magnetic, thermal, and electrical properties, e.g., by tailoring the specific ordering and the connections at the atomic scale.^[2] One natural case is the molecular crystal formed by closely packing C₆₀ with van der Waals interaction, which

while the cages and the connection region provide alternating positive and negative curvatures.^[13] Under high pressures, e.g., above 20 GPa, however, C₆₀ cages would break and form carbons with a high content of sp³ hybridization and become superhard.^[14] Zhang et al. reported narrow-gap and superhard amorphous carbon derived from C₆₀ under high pressure.^[15] Wang et al. reported an ordered amorphous carbon clusters (OACC) by crushing *m*-xylene solvated C₆₀ cages under high pressure at room temperature.^[16] Recently, Shang et al.^[17] and Tang et al.^[18] separately reported the preparation of amorphous diamond by crashing C₆₀ cages under a temperature above 1300 K and a pressure of ~30 GPa. Clearly, starting from C₆₀, one may have more opportunities to develop new carbon crystals with atomically tailorable structure and interesting properties more than those of diamond and graphite.

Though proceedings above, the experimental preparation of novel carbons from C₆₀ molecular crystals has been restricted by the insufficient development of experimental methods, as the most explorations have been carried out under harsh conditions. Considering a wide range of evolution possibilities caused by many atoms in one cage of C₆₀, a comprehensive theoretical understanding of the detailed structural evolution starting from C₆₀ is valuable. Melker et al. reported the formation pathway of fullerene from randomly distributed carbon atoms by *ab initio* molecular dynamics simulations (AIMD), figuring out that the final structure can be planar, cage, complex, or carbon pieces,

K. Ni, F. Pan, Y. Zhu
Department of Materials Science and Engineering
School of Chemistry and Materials Science
University of Science and Technology of China
96 Jin Zhai Rd., Hefei 230026, China
E-mail: nikun@ustc.edu.cn; zhuyanwu@ustc.edu.cn

 The ORCID identification number(s) for the author(s) of this article can be found under <https://doi.org/10.1002/adfm.202203894>.

DOI: 10.1002/adfm.202203894

depending on the temperature.^[19] But the high cost and comparably low efficiency of sampling of metastable structures in AIMD has hindered the further understanding of the potential energy surface (PES). Global structural search methods have been largely developed based on Monte Carlo method^[20] and its derivatives, such as basin hopping,^[21] particle swarm optimiza-

tion,^[22] and genetic algorithm (GA).^[23] For example, Lazauskas et al. used GA to perform a global search of 60 atom carbon system and successfully hit the C₆₀ fullerene structure.^[24] However, traditional global search requires an additional routine of energy calculation or geometry relaxation of generated structures, which often has to be combined with density functional

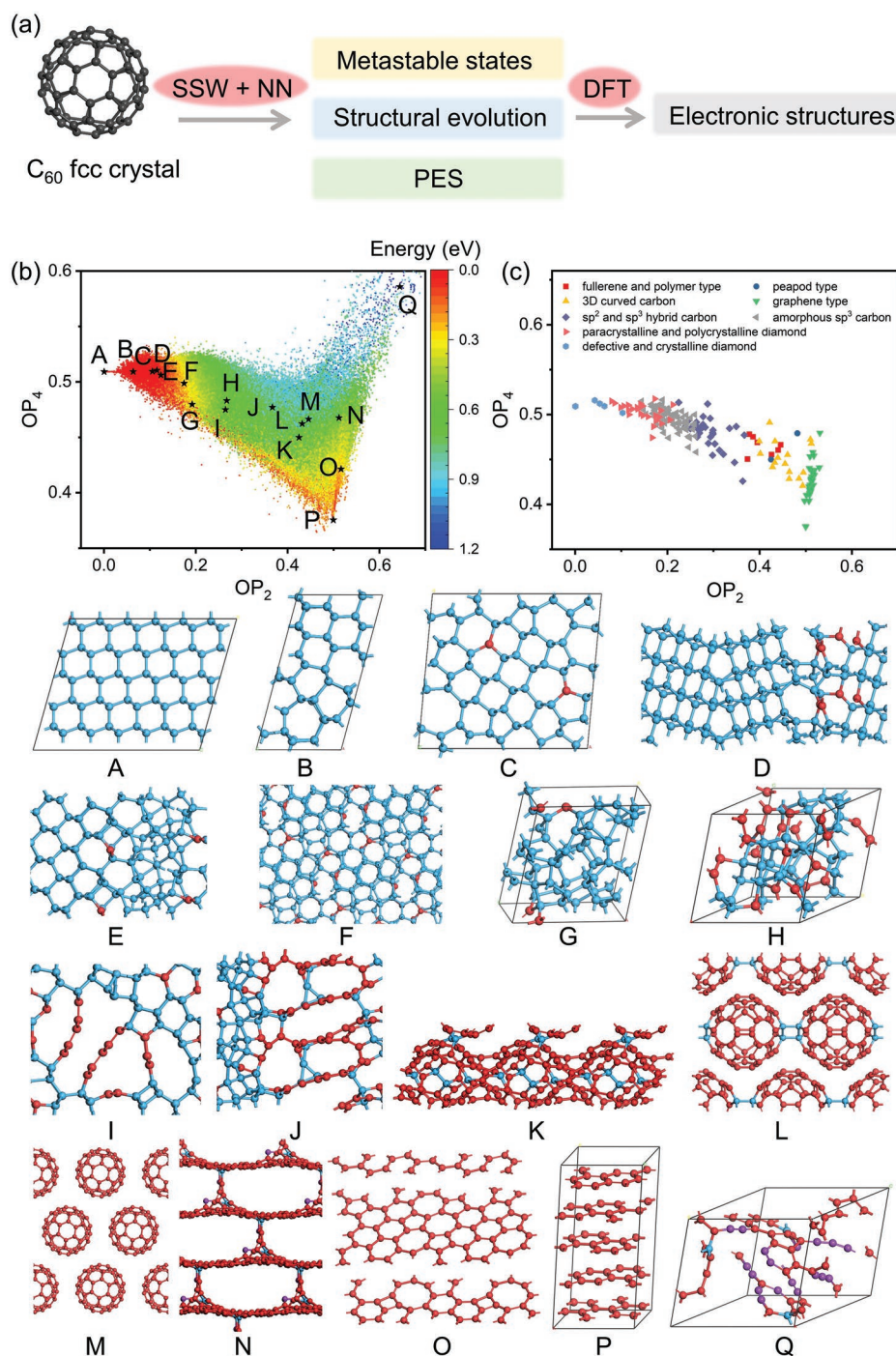


Figure 1. a) Research diagram. b) PES is defined by OP₂ and OP₄ parameters. Insets A–Q shows the typical structures in different regions in 2D PES mapping. Inset L is reported by V. A Davydov et al.^[30] Two coordinated carbon atoms are marked as purple; three coordinated carbon atoms are marked as red and four coordinated carbon atoms are marked as blue. c) Classified structural types projected into the OP₂ – OP₄ plane.

theory (DFT) methods; the high cost of DFT optimization has restricted the number of simulation atoms and the sampling coverage of PES.

On the other hand, the recently developed neural network potential (NN) method^[25] based on machine learning may greatly accelerate the speed of energy calculation while maintaining the DFT-level accuracy. Zhang et al. showed a formation of fullerene from carbon atoms using stochastic surface walking (SSW) method,^[26] demonstrating the high efficiency of SSW algorithm for searching global minimum. In addition, Zhu et al. used NN in combination of SSW method to simulate the phase transition from graphite to diamond, pointing out a favorable transition route in dynamics.^[27] In the global search of carbon isomers,^[28] however, only $10^2 \sim 10^4$ minimum states were paid attention to; the larger number (more than 10^8) of metastable states with slightly higher energy have been less discussed or totally missed.

In this work, the structural evolution starting from C_{60} fullerene crystal is systematically investigated, by combining NN and SSW methods. With Steinhardt-type order parameter (OP),^[29] the 2D PES mapping has demonstrated much more distinct types of structures than before. Under 0 GPa in the calculation, the evolutionary pathway is identified as from fullerene molecular crystal to graphite via C_{60} polymers and a large number of ordered structures with opened cages. Under a high pressure, e.g., 50 GPa, the evolution indicates the increase of sp^3 carbon bonds and eventually to crystal diamond, which

well covers the structure of amorphous diamonds recently reported.^[16–18] With DFT level study the relationship between the energy gap of metastable structures and the OP_2 geometrical descriptor is built up, providing a guidance for further experimental studies.

2. Results and Discussion

The overall research is schematically shown in **Figure 1a**. The PES of evolution was explored by SSW with energy calculation by NN potential and electronic structures calculated with DFT. A total number of 673 338 structures were sampled for PES with pressures ranging from 0 to 50 GPa, containing six repeating simulations, as shown in **Figure 1b**. For one of six simulations, more details on the PES, including averaged coordination number and sequence of structural evolution under each pressure can be found in **Figure S1–S51**, Supporting Information; the structural evolution anime can be found in **Movie S1–S51**, Supporting Information. The energy value is labeled as the relative energy to AB stacking graphite under each pressure. From the PES mapping, we can identify two low-energy regions, corresponding to graphene-type structures at OP_2 equals 0.5, and diamond-type structures at OP_2 equals 0. Some representative structures are shown in the insets of **Figure 1b**, from which we can have a glance of the structural characteristics in the 2D PES mapping, showing the geometrical correlations between local minimum states, e.g. fullerene,

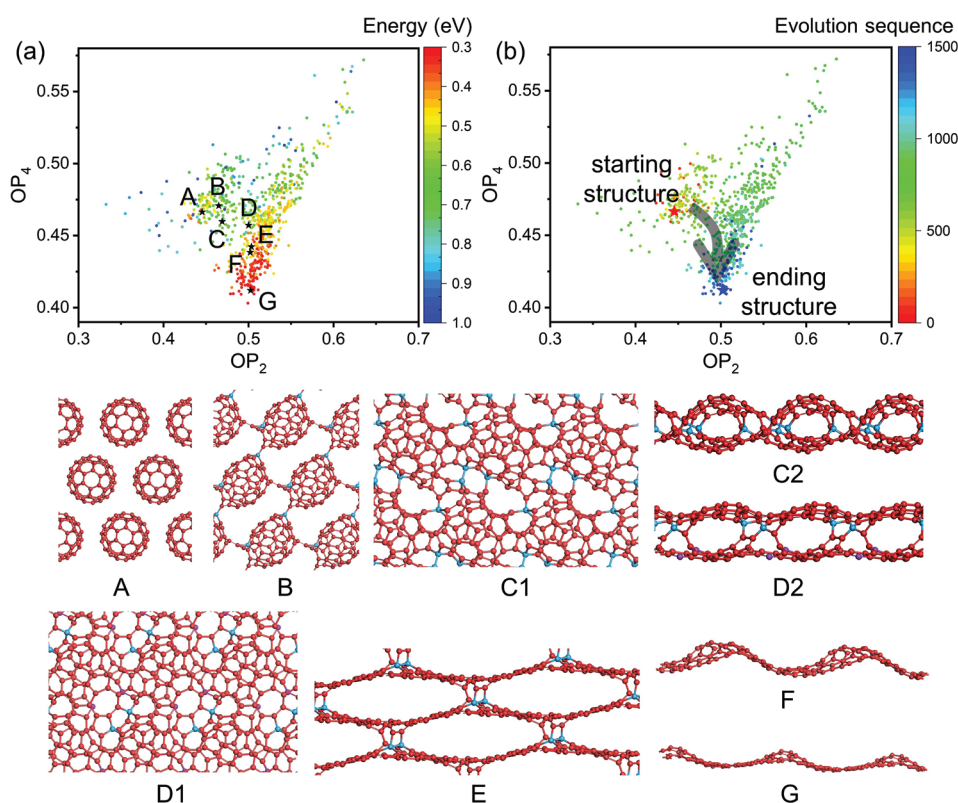


Figure 2. a) Structural evolution of C_{60} under 0 GPa in 2D PES. The color bar identifies energy relative to graphite. Insets AG shows the typical structures in different regions in the 2D PES mapping. N (1 or 2) in C_n and D_n indicates the different angles of view of C and D structures. Two coordinated carbon atoms are marked as purple; three coordinated carbon atoms are marked as red and four coordinated carbon atoms are marked as blue. b) The sequence of structural evolution corresponding to the SSW step in the calculation.

graphene, and diamond. We have also chosen one structure from every 500 structures and manually labeled the structural types in Figure 1c. The geometry of selected structures and detailed classification are shown in Figure S52–S70 and Table S1, Supporting Information, respectively. From Figure 1c, we can find typical structures, e.g., fullerene and polymer type, peapod type, 3D curved carbon, graphene type, sp^2 and sp^3 hybrid carbon, amorphous sp^3 carbon, paracrystalline and polycrystalline diamond, and defective and crystalline diamond. The clustering distribution of the same type of structures indicates that the classification based on OP parameters can efficiently divide the 2D PES plane into regions corresponding to the specific structural characteristics.

The structural evolution of C_{60} molecular crystal under 0 GPa is of vital importance to understand the intrinsic behavior of carbon atoms in the evolution. PES is calculated as relative energy to graphite, as shown in Figure 2a. We can see that the fullerene-type structures show a local minimum region with an energy of -0.4 – 0.5 eV relative to graphite, while the graphene-type structures are in the global minimum region. Insets A to G show typical structures along the evolution path. In combination of the evolution sequence in the OP_2 and OP_4 plane shown in Figure 2b, we can identify a typical structural evolution

path from fullerene to graphite: 1) Starting from fcc molecular crystal, C_{60} balls are first polymerized, as shown in Inset B; 2) Further connection between cages leads to 2D connected structures with opened cages, yet with ordering (Inset C) with a side view of curved peapods; 3) More connections lead to the larger opening, forming two curved carbon layers with less bonds between layers (Insets D and E); 4) The interlayer connections are broken, forming curved graphene layers (Inset F); 5) The curvature of the carbon plane are reduced with the repair of the in-plane topological defects (Inset G); 6) Complete repair of defects eventually leads to the formation of graphite. Obviously, the structural evolution under 0 GPa shows a direction towards increased OP_2 and decreased OP_4 . Many metastable structures, shown in the pathway of structural transition from C_{60} molecular crystal to AB graphite, indicates that one may be able to prepare more novel carbons by finely tuning the order parameter, with proper experimental strategies.

Recently, amorphous diamond or paracrystalline diamond prepared from C_{60} under high pressure and high temperature has attracted much attention,^[17,18] further showing the power of pressure in terms of obtaining new carbons. The structural evolution of C_{60} has also been investigated under 50 GPa and the 2D PES mapping is shown in Figure 3a. Starting from

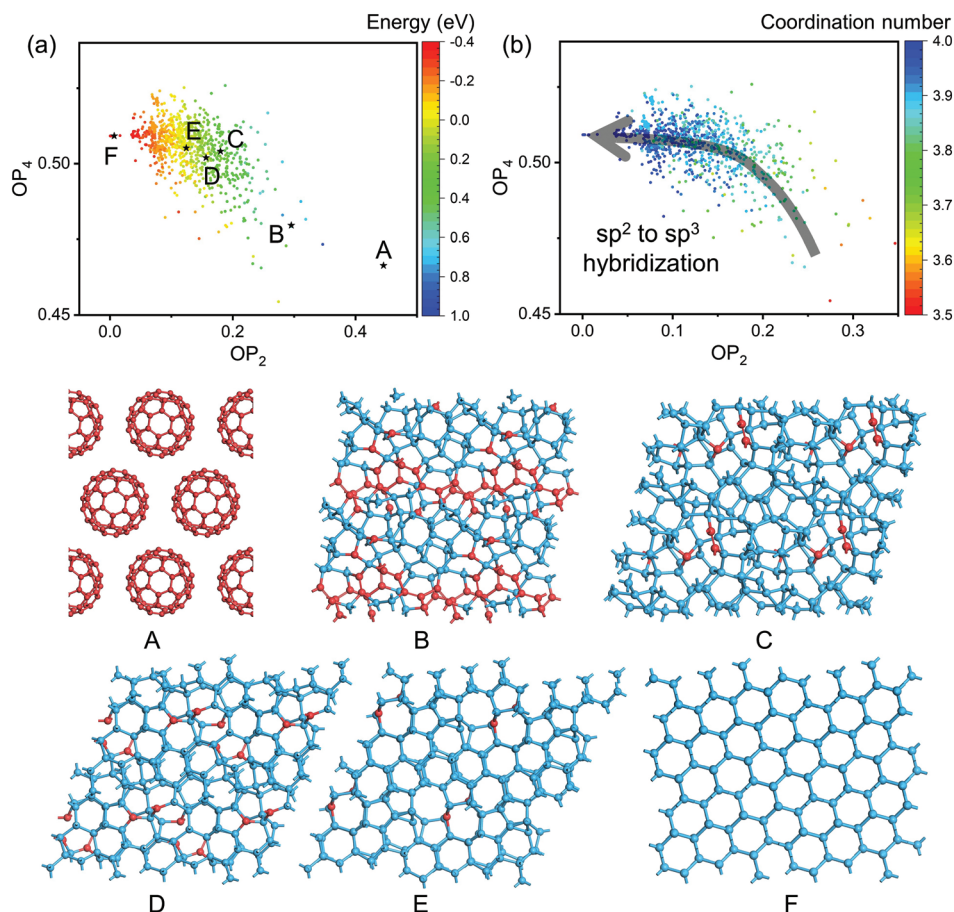


Figure 3. a) Structural evolution of C_{60} molecular crystal under 50 GPa, shown in 2D PES mapping. The color bar identifies the energy relative to that of graphite. Insets A–F shows the typical structures taken from different regions in the 2D PES mapping. Three coordinated carbon atoms are marked as red and four coordinated carbon atoms are marked as blue. b) Averaged coordination number in $OP_2 - OP_4$ plane.

C_{60} molecular crystal (Inset A), the structural evolution shows a direction towards decreased OP_2 and increased OP_4 , in contrast to the situation under 0 GPa in Figure 2b. The final structure obtained is a cubic diamond (Inset F). In the evolution, several intermediate states are shown in Insets B to E, from which we can figure out a typical evolution pathway under 50 GPa: 1) C_{60} cages crash and connect to each other, forming sp^2 and sp^3 hybrid carbon while maintaining the long-range order, as shown in Inset B, which may correspond to reported OACC structure^[16]; 2) More sp^2 components transform into sp^3 hybridization, resulting in an amorphous sp^3 carbon (Inset C), possibly related to the structure reported by Shang et al.^[17] and Zhang et al.^[14a]; 3) Crystal seeds form in sp^3 amorphous phase and grow, leading to paracrystalline diamond (Inset D), probably close to the structure reported by Tang et al.^[18]; 4) Crystal domains contact to each other, forming polycrystalline diamond or defective crystalline diamond, as shown in Inset E; 5) Repair of the defects leads to the formation of cubic crystalline diamond (Inset F). In addition, Figure 3b clearly shows the evolution of averaged coordination number with consideration of periodicity, in which coordination number 3 corresponds to sp^2 hybridization and coordination number 4 corresponds to sp^3 hybridization.

The dependence of evolution on the pressure has been investigated in detail. The final structure for each pressure is collected and projected on the OP_2 - OP_4 map, from six repeating simulations, as shown in Figure 4. The final structures under each pressure from one of six simulations are shown in Figure S71–S75, Supporting Information. In the mapping, three regions are cycled to guide the eyes, corresponding to: (A) graphene-like structural region with OP_2 values greater than 0.25; (B) amorphous carbon region with OP_2 values between 0.15 and 0.25; (C) diamond-like structural region with OP_2 values lower than 0.15. The range of OP_2 values for different structural types, e.g., between 0.15 and

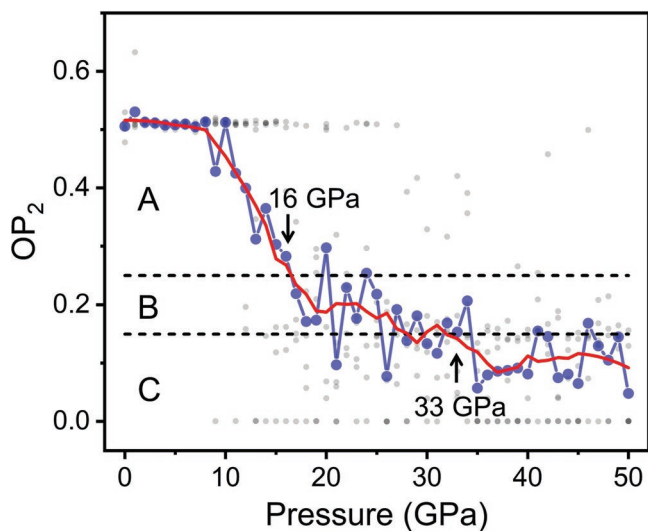


Figure 4. OP_2 values of final structures under pressures from 0 to 50 GPa. The gray dots are OP_2 values by six repeating simulations. The blue line shows the averaged OP_2 value, which is further smoothed by Savitzky–Golay method,^[31] as indicated by the red line. The dash line shows the boundary of Region A, B, and C. Two critical pressures along the directionality of structural evolution are labeled.

0.25 for amorphous carbon, can be obtained from Figure 1c. Depending on the pressure applied, we may clarify the evolution under pressures: 1) At pressures below ~ 16 GPa, the structural evolution direction is towards graphene and graphite type; 2) At the medium pressure range of between ~ 16 and ~ 33 GPa, the evolution is towards amorphous carbon; 3) At pressures above ~ 33 GPa, the evolution is directed to paracrystalline and polycrystalline diamonds. We also notice that the sampling of the structures may introduce an uncertainty of the evolution direction, due to the limited (1500) steps of random moving directions, which can be inferred by comparing the results in Figure S1–S51, Supporting Information. But the pressure-dependent evolution path is clear.

Based on the geometrical evolution obtained by SSW+NN global searching, DFT simulations have been performed to investigate the evolution of electronic structures. The band gaps of 222 labeled structures were calculated from density of states (DOS), shown in the OP_2 – OP_4 map in Figure 5. Detailed DOS results for several representative structures can be found in Figure S76–S78, Supporting Information. We can see that the band gap increases with the decrease of OP_2 parameter. As OP_2 is calculated from pure geometrical aspect, the trend in Figure 5 clearly demonstrates a structure-property relationship, i.e., an averaged hybridization-dependent electronic bandgap. The partial charge density of valence band maximum (VBM) and conduction band minimum (CBM) is shown in the inset of Figure 5 and the detailed drawing parameters are listed in Table S2, Supporting Information, showing how the electron orbital changes when the carbon system transforms from sp^2 to sp^3 hybridization. The VBM and CBM contribute to π and π^* orbitals when OP_2 is near 0.5 in sp^2 hybridized carbon, and turns to be σ and σ^* when OP_2 is near 0, corresponding to sp^3 hybridized carbon. The frequency analysis of predicted structures is shown in Table S3–S5, Supporting Information, showing no remarkable imaginary optical frequencies, indicating that the structures are stable. In addition, the predicted structures remain unchanged after AIMD simulations at 300 K for 5 ps, as shown in Figure S79–S82, Supporting Information.

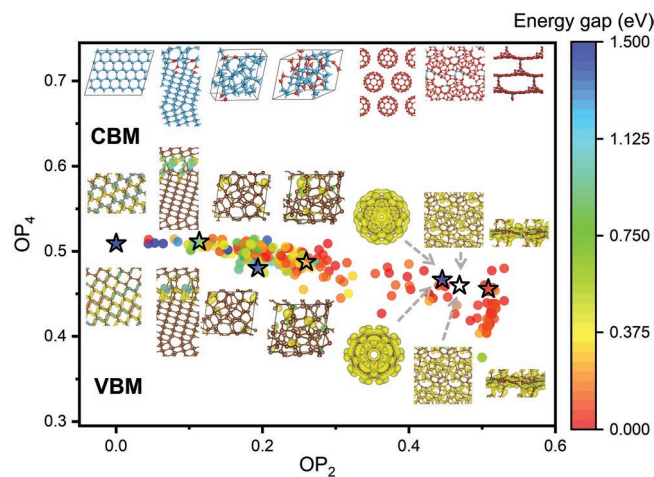


Figure 5. Energy band gaps of 222 labeled structures in OP_2 – OP_4 map. Insets show VBM and CBM for seven representative structures marked as stars.

3. Conclusion

In this work, the structural evolution starting from C₆₀ molecular crystal has been investigated by accelerating the energy calculation with neural network potential method. The PES was explored by SSW algorithm and 673 338 metastable structures were obtained, from which the transformation of C₆₀ molecular crystal into other carbons, e.g. graphite, amorphous carbon, and diamond has been described in detail. We have found that the structural evolution follows a sequence of molecular crystal → polymers → opened caged ordered structures → 3D curved carbon and graphite under 0 GPa and a pathway of fullerene → sp² and sp³ hybrid carbon → sp³ amorphous carbon and crystal diamond under 50 GPa. DFT calculations have shown that the bandgap of obtained structures decreases with OP₂ geometrical parameters. Our work gives insights into the PES starting from fullerene-based materials and may further broaden the interest of preparing novel ordered carbons from fullerene.

4. Experimental Section

The global structural search was performed using Large scale Atomic Simulation with neural network Potential software (LASP).^[32] The SSW algorithm was implemented in LASP.^[26] The NN potential of carbon was obtained from LASP website and further trained. 51 runs were performed with pressures varying from 0 to 50 GPa, with a step of 1 GPa. Each run contained 1500 SSW searching steps. To increase the possibility to hit the global minimum in each run, the structural search was done in three steps with the control of acceptance temperature (T_a). Here T_a was known as the temperature parameter in metropolis criterion.^[33] T_a equaled to 300 K in the first 500 SSW steps, and then was set to 3000 K in the next 500 SSW steps, then equaled to 300 K again in the last 500 SSW steps. T_a = 3000 K in the second 500 steps was helpful to overcome energy barriers and to reach metastable states with relatively higher energy, thus having a bigger possibility to hit the global minimum in the final structure. The above sampling was repeatedly run for six times to reduce the error by randomness. The input file of LASP calculation for 50 GPa pressure was listed below.

```
potential NN
explore_type ssw
Ewaldflag 0
%block netinfo
C C.pot
%endblock netinfo
PrintChg 0
Run_type 15
SSW.SSWsteps 1500
SSW.LowTemp 300 K
SSW.HighTemp 3000 K
SSW.TempCycle 500
SSW.pressure 50.0
SSW.quick_Setting 3
SSW.ftol 1E-2
SSW.ds_atom 1.7
SSW.output F
SSW.printevery F
SSW.printselect 0
```

Steinhardt-type order parameter (OP) was calculated by the following formula:

$$OP_l = \left(\frac{4\pi}{2l+1} \sum_{m=-l}^l |\overline{Y_{lm}(n)}|^2 \right)^{1/2} \quad (1)$$

where Y_{lm} is the spherical harmonic function of degree l and order m ; n is the normalized direction between all bonded atoms, and the bar over Y_{lm} means the average overall bonded atoms.^[29] Thus, OP parameters are obtained purely based on geometrical structure and reflect the spatial distribution of the bonded atoms in the structure. OP₂ and OP₄ values of several carbon crystals can be found in Table S6, Supporting Information. More illustrations of OP_l parameters can be found in the supporting file.

The electronic properties of obtained structures were calculated by Vienna Ab initio Simulation Package.^[34] Generalized gradient approximation^[35] with Perdew–Burke–Ernzerhof (PBE)^[36] functional was used. The basis set energy cutoff was 500 eV. Gaussian type smearing was adopted with an energy window of 0.1 eV. All calculations were done with spin unrestricted. The self-consistent field convergence criteria were 0.01 meV and the force tolerance for geometry optimization was 0.02 eV/Å. Becke–Johnson damping DFT-D3 correction^[37] was used. The gamma-centered K point sampling was done with a spacing of 0.1 Å⁻¹ for AIMD simulation, 0.04 Å⁻¹ for geometry optimization, and 0.01 Å⁻¹ for DOS calculation.

Statistical Analysis: Data were analyzed using a postprocessing python script to compute the OP_l values of the structures. The 2D PES was plotted by Origin Pro software. The geometric structures were plotted by Materials Studio software. The shell scripts were used for gathering and analyzing data from different calculation runs.

Supporting Information

Supporting Information is available from the Wiley Online Library or from the author.

Acknowledgements

This work was supported by the National Key R&D Program of China (Grant Nos. 2020YFA0711502) and the Natural Science Foundation of China (Nos. 51972299, 52003265). USTC Super Computing Center was appreciated.

Conflict of Interest

The authors declare no conflict of interest.

Data Availability Statement

The data that support the findings of this study are available from the corresponding author upon reasonable request.

Keywords

DFT calculations, fullerenes, global structural search, neural network potential

Received: April 9, 2022
Revised: June 14, 2022
Published online: August 7, 2022

- [1] E. Omacsawa, *Perspectives of Fullerene Nanotechnology*, Springer Science & Business Media, Berlin, New York, 2012.
[2] K. Chen, L. Li, *Adv. Mater.* **2019**, *31*, 1901115.

- [3] G. Van Tendeloo, S. Amelinckx, M. Verheijen, P. Van Loosdrecht, G. Meijer, *Phys. Rev. Lett.* **1992**, 69, 1065.
- [4] J. L. de Boer, S. van Smaalen, V. Petricek, M. Dusek, P. M. A. Verheijen, G. Meijer, *Chem. Phys. Lett.* **1994**, 219, 469.
- [5] M. Núñez-Regueiro, L. Marques, J.-L. Hodeau, O. Béthoux, M. Perroux, *Phys. Rev. Lett.* **1995**, 74, 278.
- [6] Y. Zhao, D. Poirier, R. Pechman, J. Weaver, *Appl. Phys. Lett.* **1994**, 64, 577.
- [7] A. Rao, P. Zhou, K. Wang, G. Hager, J. Holden, Y. Wang, W.-T. Lee, X. Bi, P. Eklund, D. Cornett, M. Duncan, I. Amster, *Science* **1993**, 259, 955.
- [8] S. Margadonna, D. Pontiroli, M. Belli, T. Shiroka, M. Ricco, M. Brunelli, *J. Am. Chem. Soc.* **2004**, 126, 15032.
- [9] R. Taylor, D. R. Walton, *Nature* **1993**, 363, 685.
- [10] S. Okada, S. Saito, A. Oshiyama, *Phys. Rev. Lett.* **1999**, 83, 1986.
- [11] E. Hernandez, V. Meunier, B. Smith, R. Rurali, H. Terrones, M. Buongiorno Nardelli, M. Terrones, D. E. Luzzi, J.-C. Charlier, *Nano Lett.* **2003**, 3, 1037.
- [12] R. Phillips, D. A. Drabold, T. Lenosky, G. B. Adams, O. F. Sankey, *Phys. Rev. B* **1992**, 46, 1941.
- [13] K. Nueangnoraj, H. Nishihara, K. Imai, H. Itoi, T. Ishii, M. Kiguchi, Y. Sato, M. Terauchi, T. Kyotani, *Carbon* **2013**, 62, 455.
- [14] a) S. Zhang, Z. Li, K. Luo, J. He, Y. Gao, A. V. Soldatov, V. Benavides, K. Shi, A. Nie, B. Zhang, W. Hu, M. Ma, Y. Liu, B. Wen, G. Gao, B. Liu, Y. Zhang, Y. Shu, D. Yu, X. Zhou, Z. Zhao, B. Xu, L. Su, G. Yang, O. P. Chernogorova, Y. Tian, *Natl. Sci. Rev.* **2022**, 9, nwab140; b) B. Sundqvist, *Phys. Rep.* **2021**, 909, 1; c) Z. Zhao, B. Xu, Y. Tian, *Annu. Rev. Mater. Res.* **2016**, 46, 383.
- [15] S. Zhang, Y. Wu, K. Luo, B. Liu, Y. Shu, Y. Zhang, L. Sun, Y. Gao, M. Ma, Z. Li, *Cell Rep. Phys. Sci.* **2021**, 2, 100575.
- [16] L. Wang, B. Liu, H. Li, W. Yang, Y. Ding, S. V. Sinogeikin, Y. Meng, Z. Liu, X. C. Zeng, W. L. Mao, *Science* **2012**, 337, 825.
- [17] Y. Shang, Z. Liu, J. Dong, M. Yao, Z. Yang, Q. Li, C. Zhai, F. Shen, X. Hou, L. Wang, N. Zhang, W. Zhang, R. Fu, J. Ji, X. Zhang, H. Lin, Y. Fei, B. Sundqvist, W. Wang, B. Liu, *Nature* **2021**, 599, 599.
- [18] H. Tang, X. Yuan, Y. Cheng, H. Fei, F. Liu, T. Liang, Z. Zeng, T. Ishii, M. Wang, T. Katsura, H. Sheng, H. Gou, *Nature* **2021**, 599, 605.
- [19] A. I. Melker, S. N. Romanov, D. A. Kornilov, *Mater. Phys. Mech.* **2000**, 2, 42.
- [20] E. Shakhnovich, G. Farztdinov, A. Gutin, M. Karplus, *Phys. Rev. Lett.* **1991**, 67, 1665.
- [21] M. Iwamatsu, Y. Okabe, *Chem. Phys. Lett.* **2004**, 399, 396.
- [22] J. Kennedy, R. Eberhart, presented at Proceedings of ICNN'95-International Conference on Neural Networks, Perth, WA, Australia, 27 November–01 December **1995**.
- [23] S. Sivanandam, S. Deepa, in *Introduction to Genetic Algorithms*, Springer, Berlin, New York, **2008**
- [24] T. Lazauskas, A. A. Sokol, S. M. Woodley, *Nanoscale* **2017**, 9, 3850.
- [25] S. Huang, C. Shang, X. Zhang, Z. Liu, *Chem. Sci.* **2017**, 8, 6327.
- [26] X. Zhang, C. Shang, Z. Liu, *J. Chem. Theory Comput.* **2013**, 9, 3252.
- [27] S. Zhu, Q. Hu, *Phys. Chem. Chem. Phys.* **2021**, 23, 20560.
- [28] B. Karasulu, J.-M. Leyssale, P. Rowe, C. Weber, C. de Tomas, *Carbon* **2022**, 191, 255..
- [29] P. J. Steinhardt, D. R. Nelson, M. Ronchetti, *Phys. Rev. B* **1983**, 28, 784.
- [30] V. Davydov, L. Kashevarova, A. Rakhmanina, V. Senyavin, R. Ceolin, H. Szwarc, H. Allouchi, V. Agafonov, *Phys. Rev. B* **2000**, 61, 11936.
- [31] W. H. Press, S. A. Teukolsky, *Comput. Phys.* **1990**, 4, 669.
- [32] S. Huang, C. Shang, P. Kang, X. Zhang, Z. Liu, *Wiley Interdiscip. Rev.: Comput. Mol. Sci.* **2019**, 9, e1415.
- [33] P. J. Van Laarhoven, E. H. Aarts, in *Simulated Annealing: Theory and Applications*, Springer, Berlin, New York, **1987**.
- [34] J. Hafner, *J. Comput. Chem.* **2008**, 29, 2044.
- [35] J. P. Perdew, K. Burke, M. Ernzerhof, *Phys. Rev. Lett.* **1996**, 77, 3865.
- [36] M. Ernzerhof, G. E. Scuseria, *J. Chem. Phys.* **1999**, 110, 5029.
- [37] S. Grimme, J. Antony, S. Ehrlich, H. Krieg, *J. Chem. Phys.* **2010**, 132, 154104.